

Rheology of hydrating cement paste: crossover between two aging processes

Atul Varshney^{a,b,*}, Smita Gohil^{a,*}, B. A. Chalke^a, R. D. Bapat^a, S. Mazumder^c, S. Bhattacharya^a, Shankar Ghosh^{a,*}

^a*Department of Condensed Matter Physics and Materials Science, Tata Institute of Fundamental Research, Homi Bhabha Road, Mumbai 400 005, India*

^b*Department of Physics of Complex Systems, Weizmann Institute of Science, Rehovot, Israel 76100*

^c*Solid State Physics Division, Bhabha Atomic Research Centre, Mumbai 400 085, India*

Abstract

The roles of applied strain and temperature on the hydration dynamics of cement paste are uncovered in the present study. We find that the system hardens over time through two different aging processes. The first process dominates the initial period of hydration and is characterized by the shear stress σ varying sub-linearly with the strain-rate $\dot{\gamma}$; during this process the system is in a relatively low-density state and the inter-particle interactions are dominated by hydrodynamic lubrication. At a later stage of hydration the system evolves to a high-density state where the interactions become frictional, and σ varies super-linearly with $\dot{\gamma}$; this is identified as the second process. An instability, indicated by a drop in σ , that is non-monotonic with $\dot{\gamma}$ and can be tuned by temperature, separates the two processes. Both from rheology and microscopy studies we establish that the observed instability is related to fracture mechanics of space-filling structure.

Keywords: Cement paste, Hydration, Rheology, Microstructure, Aging

1. Introduction

Hardening process of cement in the presence of water has been a subject of research besides its industrial importance [1]. Cement paste, usually a dense suspension of non-Brownian particles, exhibits complex rheological properties that depend on several factors including particles' shape and size, cement composition, cement/water ratio, measurement methods etc [2, 3, 4]. In the presence of water, ordinary portland cement (OPC) – a commonly used binding agent – forms gel-like structure that arises predominantly from the chemical reactions producing calcium-silicate-hydrates (C-S-H) [5, 6, 7]. Besides C-S-H, aluminates – a fast reacting phase present in OPC – form space filling needle-like structures called Ettringites. This is accompanied with the growth of a cohesive system-spanning network of C-S-H which bridges the hydrating cement grains. As a result stress-bearing submicron structures form in the system which offer resistance in response to applied shear. The Ettringites, however, contribute to the solidification of cement only during its initial stage of hydration [1].

As the hydration reaction proceeds over time, the morphology of the C-S-H network grows in a manner that gives rise to an overall decrease of pore density and relatively a compact structure evolves [4, 8]. With the availability

of water running out the interparticle interactions in this stage of hydration are mainly frictional in nature [5, 9]. Hardening of the system at long times is analogous to the ubiquitous phenomena of aging observed in frictional systems [10]. It relates to the reconstruction of the interfacial contact zones [10, 11] and flow induced reconfigurations of its constituents, such that, a low density cluster of particles which has fewer contacts with its neighbors evolves into a denser structure that shares more contacts with its neighbors [12, 13, 14].

Aggregation and network formation are out-of-equilibrium phenomena that are commonly influenced by mechanical perturbations, e.g., shear flow [3, 15, 16]. Such perturbations would lead to mechanical failure [17] at multiple length scales., e.g., at the scale of the contact region between the particles it is related predominantly to the breaking of the calcium-silicate-hydrate bonds while at larger scale it relates to the shear-induced transformation of particle configurations [15]. However, most studies that address the issues related to the emergence of mechanical strength in cement paste have been performed in the presence of small external stresses that perturb the system about a local minima of its potential energy landscape [1, 16, 18, 19].

Temperature plays multiple roles; it enhances the rate of hydration [9], determines the filling of the interstitial space between the grains and allows thermally activated processes to release the internal stresses *via* creep [20, 21]. Arguments in similar lines are usually proposed to understand the variation of the mechanical properties of cement on its curing temperature [20, 22]. Cement cured at

*Corresponding author

Email addresses: atul.varshney@weizmann.ac.il (Atul Varshney), smitagohil@tifr.res.in (Smita Gohil), sghosh@tifr.res.in (Shankar Ghosh)

low temperatures develops a more compact structure with improved mechanical stability through a slow and controlled process of filling up the interstitial space between the cement grains. In contrast, curing at high temperature produces non-uniform structure with low compressive strengths [22, 23].

In this paper we study the hardening process of cement paste as a function of temperature and in presence of large-scale mechanical perturbations (large oscillatory shear) where the imposed shear disrupts the energy landscape by constantly restructuring the interwoven matrix of hydrate needles. We observe that the cement paste gains shear rigidity via two distinct aging processes; the first aging process is associated with the *setting* process that generates space-filling structures (e.g., Ettringite needles) and provides the system its initial rigidity. This system has flow curves that show shear-thinning behavior. In contrast, the second process is associated with the *hardening* phenomena that arises from the formation of C-S-H networks and the material manifests shear-thickening behavior. In addition, the crossover from the first to the second aging process occurs through a global weakening in the system, indicated by a drop in the measured shear stress. We also show that with lowering temperature the drop occurs later in time and its magnitude decreases. Both these phenomena are related to the reaction kinetics of the hydrates formation. Finally, we establish that the weakening is related to the fracture mechanics of the space-filling structure formed during the initial phase of cement hydration.

2. Experiment

In experiments, we use a cement paste prepared by mixing OPC (c) with deionized water (w) in a ratio $w/c = 0.5$ for about a minute and then immediately transferred to the rheometer for measurements [24]. This water to OPC ratio allows us to access the hydrodynamic lubrication regime between the cement grains during its initial phase of hydration. We also perform the rheological measurements on Alite paste, prepared in the same water to cement ratio, and compare the data with that of OPC. Alite (C_3S ; tricalcium silicate) – a major phase present in the cement – is believed to contribute primarily to the mechanical strength of hydrating cement paste through formation of C-S-H; it does not produce Ettringites [7, 25, 26].

2.1. Microscopy

The scanning electron micrographs in Fig. 1 capture the evolution in the morphology of the cement particles during the process of hydration at temperature $T = 30^\circ\text{C}$. In the early stage of hydration, Ettringite (calcium sulfoaluminate hydrate) forms, which is a faster growing compound and can be seen as needle-shaped structures in Fig. 1(b-d), and primarily occupies more volume in the system.

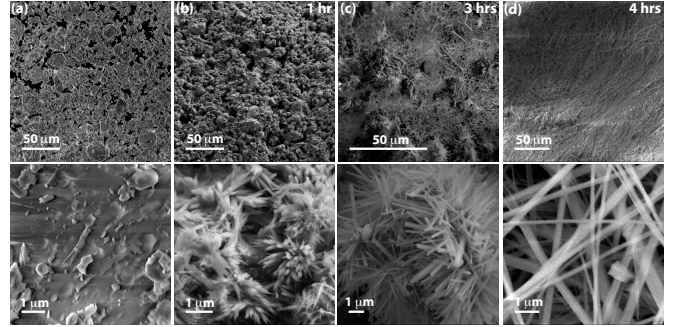


Figure 1: (a) Scanning electron micrographs of dry cement powder grains. (b-d) Low (top panel) and high (bottom panel) magnification micrographs of hydrated cement at 30°C with $t = 1$ hr, 3 hrs and 4 hrs, respectively. The interweaved needle structure and its growth with time are evident in the high magnification images.

2.2. Oscillatory Rheology

A conventional strain-controlled rheometer (MCR301; Anton Paar) is used to perform oscillatory rheological measurements of the cement paste as a function of time t and at various temperatures T . The cement paste is subjected to a sinusoidal shear strain of amplitude γ at a fixed oscillation frequency ω and correspondingly waveform of torque is being recorded by the rheometer. Typically the time varying angular displacement of the measuring device and the measured torque are converted to strain and shear stress, respectively by multiplying them with suitable ‘form factors’ which are specific to a given measuring system. However, the conversion from angular displacement to strain is obtained by assuming a linear velocity profile in the measurement gap region and no-slip conditions at the walls. For some applications this assumption may not strictly hold, e.g., avalanche motion in sand piles is a surface phenomenon where the particulate matter screens the stress such that only a shallow region close to the moving surface is sheared [27]. For these systems both shear stress and strain are underestimated by the rheometer [28].

The measurements are done in two methods: (1) a parallel-plate geometry is used (see schematic in Fig. 2(a)) and oscillatory strain of amplitude $\gamma = 1\%$ at $\omega = 6.28$ rad/s is applied to the cement paste. The process of hardening of the cement paste is monitored by measuring the amplitude σ of the waveform associated to the shear stress as a function of hydration time (t). The measurement is repeated on fresh cement paste for different gap height h between the parallel plates at $T = 30^\circ\text{C}$, and for different T at a fixed gap $h = 2$ mm. Grounded glass plate (radius $R = 25$ mm) is used as the shearing surface to ensure sustained contact with the cement paste. The strain amplitude (γ) is measured at the circumference of the top plate through $\gamma = R\phi/h$, where ϕ is the angular displacement. (2) a concentric cone-cylinder geometry (cone radius $r_1 = 13.3$ mm, cylinder radius $r_2 = 14.5$ mm, cone angle= 120°) is used to measure a set of flow curves, i.e., σ versus $\dot{\gamma}$, at $\omega = 1$ rad/s and at time intervals of

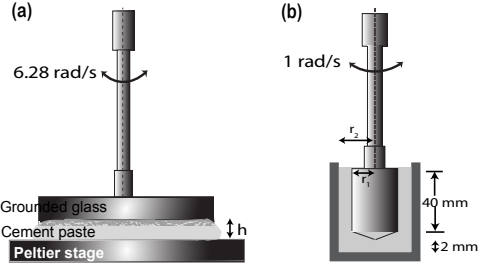


Figure 2: Schematics of measurement geometries (not to scale): (a) parallel-plate (b) concentric cone-cylinder.

1 hr while the system is maintained at a constant T . The strain-rate ($\dot{\gamma}$) in this geometry is equal to the amplitude of $(\frac{r_2^2+r_1^2}{r_2^2-r_1^2})(\frac{d\phi}{dt})$. A schematic of the cone-cylinder geometry is shown in Fig. 2(b).

3. Results and discussion

In this section we first report our experimental observations in the parallel-plate geometry and later provide a detailed account of observed phenomena in the cone-cylinder geometry.

3.1. Parallel-plate geometry

(a) Temporal evolution of shear stress

Figure 3(a) shows a typical variation of σ with t , obtained for $\gamma = 1\%$ and at $T = 30^\circ\text{C}$. The increase in σ above t_0 is followed by a pronounced drop ($\Delta\sigma$) at $t = t^*$ (and $\sigma = \sigma^*$). It suggests that the system begins to weaken at $t = t^*$ and regains its strength later. The weakening of the structure can come about by the initiation of bulk flows in the system. Such flows would result in a large-scale re-configuration via the alteration of the space-filling matrix brought by the applied shear [29]. In our experiments, we find $\gamma = 0.1\%$ is not effective to disrupt the structure hence σ grows with t at $T = 30^\circ\text{C}$, shown in the inset of Fig. 3(a), which is in agreement with results reported in ref. [18, 25]. As the hydration reaction proceeds, the density of cohesive C-S-H network increases [9], as a result σ regains, but with a faster rate.

The above observations are corroborated by the measurement of the phase angle (δ) between waveforms of shear stress and strain. For viscoelastic fluids, δ varies between 0 (purely elastic response) and $\pi/2$ (purely viscous response) [2]. Figure 3(b) shows the time evolution of $\tan\delta$ that increases till the point system weakens, thus it is suggestive of enhanced viscous response of the system. As the system regains its strength, $\tan\delta$ decreases with t , which indicates the subsequent growth of load bearing percolating C-S-H networks in the system. Strikingly, the value of $\tan\delta$ at long times is considerably smaller than its value at initial times which signifies the growing solid-like behavior in the system (see also Fig. 3(b) inset for different γ).

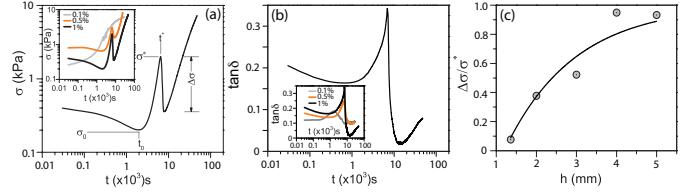


Figure 3: Variations of σ and $\tan\delta$ with hydration time (t) at $T = 30^\circ\text{C}$ and $\gamma = 1\%$ are plotted in (a) and (b), respectively. The insets to (a) and (b) compare the time variation of σ and $\tan\delta$, respectively for $\gamma = 0.1\%$ (gray), 0.5% (orange) and 1% (black), at $T = 30^\circ\text{C}$. (c) Variation of $\Delta\sigma$ normalized with σ^* for different gaps h . Solid line is a guide to the eye.

The advantage of using parallel-plate geometry is that the gap between the two plates can be adjusted. We find that the drop in shear stress ($\Delta\sigma$) normalized with its peak value (σ^*) increases initially with the gap height h and then saturates to a value close to unity, as shown in Fig. 3(c). This shows that the drop observed in σ (Fig. 3(a)) is due to the volumetric disintegration of the structures. To verify the occurrence of the stress drop, rheological measurements are performed on Alite paste at $T = 18^\circ\text{C}$. We find that $\Delta\sigma$ for Alite is about an order of magnitude smaller than that for OPC, as shown in the inset of Fig. 4(a). Thus the weakening of the system, i.e., the presence of $\Delta\sigma$ in OPC, arises due to the disruption of the space-filling structure.

(b) Role of temperature

To further study the dependency of stress drop on the rate of structure formation we perform the rheological measurements at different constant temperatures. Figure 4(a) demonstrates the time evolution of σ for various T . The ensuing growth of σ with t is not only delayed with lowering of temperature, its behavior also changes qualitatively. The drop in the stress ($\Delta\sigma$) gets progressively less pronounced with lowering of temperature (see Fig. 4(a)). The hydration rate determines the peak position, i.e., t^* , which occurs later in time with decreasing T (see Fig. 4(b)). A faster rate of growth would indeed produce a higher density of hydrates over a given period of time and vice versa [9]. The drop in σ , proportional to the number of failure events, is related to the density of hydrates and hence $\Delta\sigma$ is expected to increase with T . This is indeed the case shown in Fig. 4(c).

(c) Evidence of two aging processes

The difference in the asymptotic variations of σ with T for $t_0 < t < t^*$ and $t \gg t^*$ is illustrated in Fig. 5. Here we scale the various $\sigma - T$ graphs in the region $t > t_0$. The scaling is obtained by shifting the origin of the plots to (σ_0, t_0) and then scaling the ordinate, i.e., $(\sigma - \sigma_0)$ by $\Delta\sigma$ and the abscissa, i.e., $(t - t_0)$ by a scaling parameter τ . The temperature variation of τ is shown in the inset of Fig. 5. In a manner similar to most thermally activated

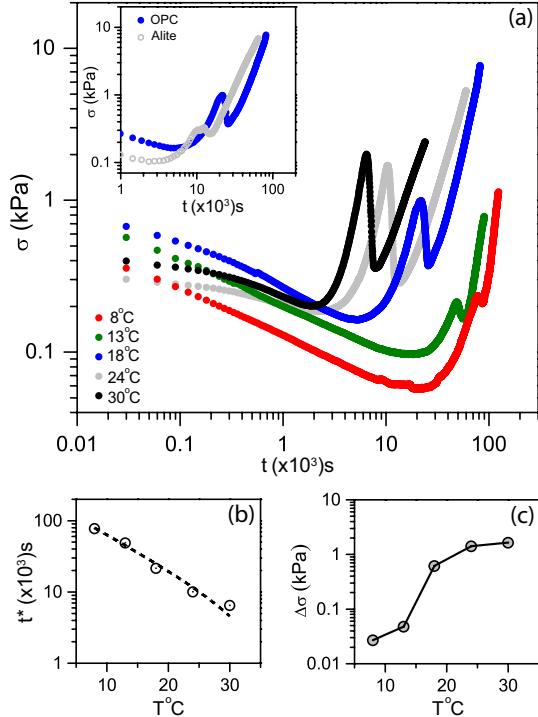


Figure 4: (a) Time evolution of σ at $\gamma = 1\%$ and for different T . Inset shows the variation of σ with t for Alite (gray) and OPC (blue) measured at 18°C . (b) Variation of t^* with T ; dashed line is an exponential fit to the data. (c) Stress drop ($\Delta\sigma$) versus T .

processes [30], τ decays exponentially with T , and one obtains an energy scale $U \sim 0.5$ eV after fitting the variation to the Arrhenius form $\tau \sim e^{-U/k_B(273+T)}$, where k_B is the Boltzmann constant.

The scaling graph illustrates the existence of two processes, shown by dashed lines in Fig. 5, via which the aging proceeds. The weakening is related to the crossover between the two processes. For smaller values of $(t-t_0)/\tau$, the rate of aging is faster in process II as compared to process I. However, the aging rate for the process I catches up with process II only later and thus the magnitude of weakening gets smaller further along the abscissa. In the context of cement, I and II correspond to the *setting* and *hardening* processes, respectively [19].

3.2. Cone-cylinder geometry

Flow curves: crossover from shear thinning to thickening

To explore further the crossover from process I to process II, we record flow curves, σ versus $\dot{\gamma}$ at a frequency $\omega = 1$ rad/s and at time intervals of one hour in the cone-cylinder geometry at $T = 8^\circ\text{C}$. Two representative flow curves for $t = 10^3$ s (open circles) and $t = 10^5$ s (filled circles) are shown in Fig. 6(a). The flow curves fit well to the general Herschel-Bulkley (HB) form [1, 31], $\sigma = \sigma_Y + A\dot{\gamma}^n$, where σ_Y is the yield stress, strain-rate $\dot{\gamma} = \omega\gamma$, A and n are additional fitting parameters, see Fig. 6(a). For $n = 1$, the material behaves like a Bingham plastic that flows like a Newtonian liquid ($\sigma \propto \dot{\gamma}$) above σ_Y [32]. For $n < 1$

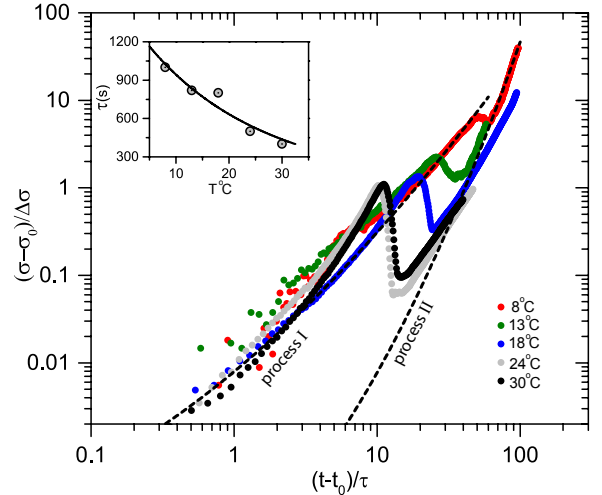


Figure 5: Scaling plot, $(\sigma - \sigma_0)/\Delta\sigma$ with $(t - t_0)/\tau$ for various T , shows the existence of two processes (highlighted by dashed lines) of aging. Here τ is a scaling parameter whose variation with T is shown in the inset. The solid line is an exponential fit of the form $\tau \sim e^{-U/k_B(273+T)}$, which yields $U \sim 0.5$ eV.

and $n > 1$ the system softens or stiffens, i.e., offers lower or higher differential resistance to flow with increasing $\dot{\gamma}$, respectively. With time the value of n crosses from $n < 1$ (shear-thinning) to $n > 1$ (shear-thickening), see Fig. 6(b). The crossover occurs at $t \sim 60 \times 10^3$ s and it is coincident with the drop in σ for $T = 8^\circ\text{C}$ (see Fig. 4(a)). It is also reflected in the time evolution of stacked flow curves, plotted in Fig. 6(c) and in the variation of $\tan \delta$ with $\dot{\gamma}$ for different t (Fig. 6(d)).

The crossover from shear thinning to thickening is also accompanied by qualitative change in the nature of the $\tan \delta - \dot{\gamma}$ curves (Fig. 6(d)). At early stages of hydration, the variation of $\tan \delta$ remains flat for low $\dot{\gamma}$ and increases with $\dot{\gamma}$ for $\dot{\gamma} \gtrsim 0.02$ s $^{-1}$. The increase in $\tan \delta$ is related to the enhanced viscous dissipation in the system that arises due to the strain-induced flow. However, at later stages of hydration and beyond $\dot{\gamma} \sim 0.3$ s $^{-1}$, $\tan \delta$ decreases with $\dot{\gamma}$ which is an indication of growing solid-like response of the system. In this stage, transient load bearing C-S-H structures form stochastically in the system and the interparticle interactions evolve to frictional type [5]. Thus, we interpret the crossover of n (Fig. 6(b)) as a signature of the time evolution of inter-particle interactions [6, 33]. For small times, it is of the lubrication type formed by the presence of water and shear-induced fluidized hydrates in the interstitial spaces between the cement particles, however, at later times with the water being converted into hydration products the interparticle interactions are mainly dominated by frictional interactions [5].

During the process of obtaining the flow curves, the system is subjected to increasing values of strain which causes failure of space-filling and C-S-H structures. Thus, the flow properties of the system at any point during the experiment is determined by the competitive dynamics of

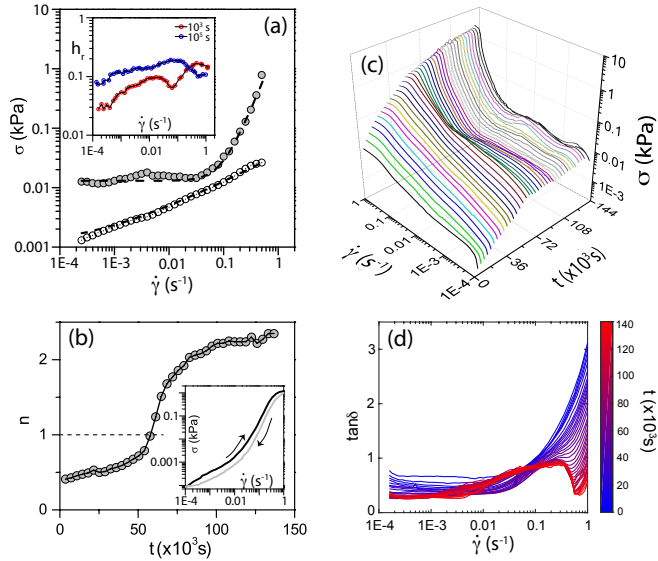


Figure 6: (a) Representative flow curves, σ versus $\dot{\gamma}$, at $\omega = 1$ rad/s and $T = 8^\circ\text{C}$, for $t = 10^3\text{s}$ (open circles) and $t = 10^5\text{s}$ (filled circles). The dashed lines are fit to the Herschel-Bulkley form. The fit yields $n = 0.47$, $\sigma_Y = 1$ kPa, $A = 4$ kPa \cdot s $^{0.47}$ for $t = 10^3\text{s}$ and $n = 2.2$, $\sigma_Y = 13$ kPa, $A = 0.1$ kPa \cdot s $^{2.2}$ for $t = 10^5\text{s}$. The inset shows variation of h_r with $\dot{\gamma}$ for two typical waveforms at $t = 10^3\text{s}$ (red) and $t = 10^5\text{s}$ (blue). (b) Variation of exponent n with t . Inset shows a typical $\sigma - \dot{\gamma}$ hysteresis curve obtained at $t = 10^5\text{s}$. (c) Stacked plot of $\sigma - \dot{\gamma}$ curves obtained at $T = 8^\circ\text{C}$; each curve is recorded at an interval of 1 hour. (d) Plot of $\tan \delta - \dot{\gamma}$ curves obtained at $T = 8^\circ\text{C}$; each curve is recorded at an interval of 1 hr. The colormap shown beside displays the hydration time t ; blue signifies the early stage of hydration and red to the later times.

the strain-induced mechanical failures and the hydration-induced growth of the load bearing C-S-H networks in the system. Further, during each flow curve the system is subjected to a large extent of deformation, i.e., $\gamma \sim 100\%$ or $\dot{\gamma} \sim 1$ s $^{-1}$. Therefore, the resulting flow erases all memory of earlier configurations and produces a fresh state of the system at the end of each strain cycle [15, 34, 35]. Moreover, at the macroscopic scale the system is almost reversible under strain cycling which is evident from a minor hysteresis loop of $\sigma - \dot{\gamma}$, shown in the inset of Fig. 6(b).

The nonlinearity in the measurements is quantified by computing the total harmonic distortion (h_r) from the recorded torque waveforms [28]. The total harmonic distortion is defined as $h_r = \sqrt{(M_2^2 + M_3^2 + \dots)}/M_1$; where M_1, M_2, M_3, \dots are the amplitudes of first, second, third, ... harmonic components of M , respectively [36]. In our experiments, we considered up to seven harmonics. The inset of Fig. 6(a) shows the variation of h_r with $\dot{\gamma}$ for $t = 10^3\text{s}$ and 10^5s . The overall distortion increases as the system evolves in time from shear thinning to thickening type, however their variation with $\dot{\gamma}$ remain almost flat (Fig. 6(a) inset).

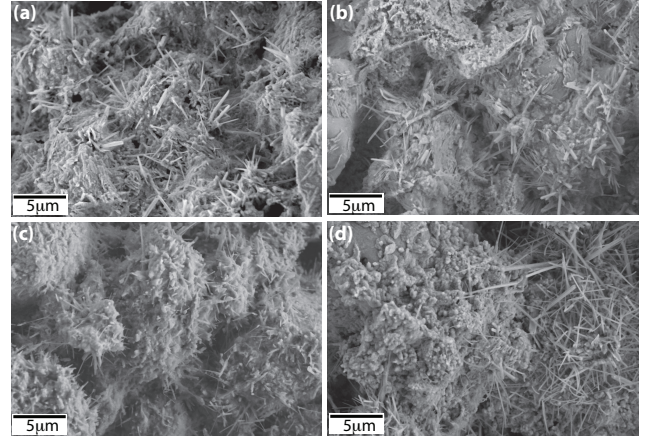


Figure 7: (a-d) Scanning electron micrographs of cement paste sheared at 30°C for ~ 4 hrs at different gaps $h = 1.3$ mm, 2 mm, 4 mm and 5 mm, respectively. To compare with similarly aged un-sheared paste, see Fig. 1(d).

3.3. Microscopic evidence of disruption of space-filling structure

Our assertion by comparing the time evolution of σ for Alite and OPC (see Fig. 4(a) inset) that $\Delta\sigma$ is associated with the fracture mechanics of the space-filling structure is supported by micrographs obtained for cement paste that has been sheared for ~ 4 hrs at 30°C shown in Fig. 7. The structures seen in the sheared paste are smaller than that observed for similarly aged un-sheared paste, see Fig. 1(d).

4. Conclusions

In conclusion, we present results from rheology of cement paste when subjected to a large amplitude shear: (i) time evolution under constant shear shows a drop in shear stress, i.e., $\Delta\sigma$, for $\gamma \geq 0.5\%$. (ii) lowering of temperature delays the onset of growth of σ ; $\Delta\sigma$ becomes less pronounced. (iii) two processes are identified *via* which the aging proceeds; process **I** corresponds to the lubrication dominated regime and process **II** to the friction dominated one. The weakening, $\Delta\sigma$, is related to the crossover between the processes. (iv) the flow curves in process **I** reveal the shear-thinning behavior of material while those in process **II** show shear-thickening. (v) large strains produce long-range particle rearrangements and as a consequence disrupts the fabric nature of the space-filling structure, as seen from the microscopy results of the cement paste that has been sheared for several hours.

Thus, we show that mechanical perturbations irrevocably alter the interwoven fabric of space-filling structure, resulting in weakening of the system. The transition *via* weakening between the two observed processes bears similarities to the structural phase transitions identified in amorphous materials and are related to local plastic deformations that often condensate to form a global soft mode

[37]. For example, in network glasses the weakening is related to the local topological rearrangements of the atoms [38, 39, 40, 41] while for particle rafts it is attributed to the compression-induced changes in the interparticle interactions that evolve from capillary bridge type to the frictional one [42]. Similar crossover from viscosity dominated lubrication regime to the frictional one has been a subject of interest in dense granular flows and suspensions [14, 42, 43, 44, 45].

References

- [1] N. Roussel (Ed.), *Understanding the rheology of concrete*, Woodhead Publ, Oxford, 2012.
- [2] R. G. Larson, *The structure and rheology of complex fluids*, Oxford University Press, New York, 1999.
- [3] R. Lapasin, V. Longo, S. Rajgelj, Thixotropic behaviour of cement pastes, *Cem. Concr. Res.* 9 (3) (1979) 309–318.
- [4] D. Lootens, P. Hébraud, E. Lécolier, H. Van Damme, Gelation, Shear-Thinning and Shear-Thickening in Cement Slurries, *Oil Gas Sci. Technol.* 59 (1) (2004) 31–40.
- [5] J. Yammine, M. Chaouche, M. Guerin, M. Moranville, N. Roussel, From ordinary rheology concrete to self compacting concrete: A transition between frictional and hydrodynamic interactions, *Cem. Concr. Res.* 38 (7) (2008) 890–896.
- [6] G. Schmidt, E. Schlegel, Rheological characterization of C-S-H phases-water suspensions, *Cem. Concr. Res.* 32 (4) (2002) 593–599.
- [7] H F W Taylor, *Cement Chemistry*, Thomas Telford Ltd, 1997.
- [8] J. J. Beaudoin, R. F. Feldman, P. J. Tumidajski, Pore structure of hardened portland cement pastes and its influence on properties, *Adv. Cem. Based Mater.* 1 (5) (1994) 224–236.
- [9] E. Gallucci, X. Zhang, K. Scrivener, Effect of temperature on the microstructure of calcium silicate hydrate (C-S-H), *Cem. Concr. Res.* 53 (2013) 185–195.
- [10] A. Ruina, Slip instability and state variable friction laws, *J. Geophys. Res.* 88 (B12) (1983) 10359.
- [11] Q. Li, T. E. Tullis, D. Goldsby, R. W. Carpick, Frictional ageing from interfacial bonding and the origins of rate and state friction, *Nature* 480 (7376) (2011) 233–236.
- [12] E. Brown, H. M. Jaeger, Shear thickening in concentrated suspensions: phenomenology, mechanisms and relations to jamming, *Rep. Prog. Phys.* 77 (4) (2014) 046602.
- [13] Y. Bai, B. Dodd, *Adiabatic Shear Localization: Occurrence, Theories and Applications*, 1st Ed., Pergamon Pr, 1992.
- [14] J. S. Langer, Shear-transformation-zone theory of plastic deformation near the glass transition, *Phys. Rev. E* 77 (2) (2008) 021502.
- [15] N. Roussel, G. Ovarlez, S. Garrault, C. Brumaud, The origins of thixotropy of fresh cement pastes, *Cem. Concr. Res.* 42 (1) (2012) 148–157.
- [16] N. Roussel, Rheology of fresh concrete: from measurements to predictions of casting processes, *Mater. Struct.* 40 (10) (2007) 1001–1012.
- [17] P. Sollich, F. Lequeux, P. Hébraud, M. Cates, Rheology of Soft Glassy Materials, *Phys. Rev. Lett.* 78 (10) (1997) 2020–2023.
- [18] M. Bellotto, Cement paste prior to setting: A rheological approach, *Cem. Concr. Res.* 52 (2013) 161–168.
- [19] L. Nachbaur, J. C. Mutin, A. Nonat, L. Choplin, Dynamic mode rheology of cement and tricalcium silicate pastes from mixing to setting, *Cem. Concr. Res.* 31 (2) (2001) 183–192.
- [20] I. Elkhadiri, M. Elkhadiri, F. Puertas, Effect of curing temperature on cement hydration, *Ceram. Silik.* 53 (2) (2009) 65–75.
- [21] P. Coussot, Q. D. Nguyen, H. T. Huynh, D. Bonn, Avalanche Behavior in Yield Stress Fluids, *Phys. Rev. Lett.* 88 (17) (2002) 175501.
- [22] I. Elkhadiri, F. Puertas, The effect of curing temperature on sulphate-resistant cement hydration and strength, *Constr. Build. Mater.* 22 (7) (2008) 1331–1341.
- [23] J. J. Beaudoin, R. F. Feldman, P. J. Tumidajski, Pore structure of hardened portland cement pastes and its influence on properties, *Adv. Cem. Based Mater.* 1 (5) (1994) 224–236.
- [24] S. Mazumder, D. Sen, A. K. Patra, S. A. Khadilkar, R. M. Cursetji, R. Loidl, M. Baron, H. Rauch, Temporal evolution of mesoscopic structure and dynamical scaling of the structure factor of some non-Euclidean systems, *Phys. Rev. B* 72 (22) (2005) 224208.
- [25] L. Nachbaur, J. Mutin, A. Nonat, L. Choplin, Dynamic mode rheology of cement and tricalcium silicate pastes from mixing to setting, *Cem. Concr. Res.* 31 (2) (2001) 183–192.
- [26] P. Barnes, J. Bensted, *Structure and Performance of Cements*, 2nd Ed., CRC Press, 2002.
- [27] A. P. F. Atman, P. Brunet, J. Geng, G. Reydellet, P. Claudin, R. P. Behringer, E. Clément, From the stress response function (back) to the sand pile “dip”, *Eur. Phys. J. E* 17 (1) (2005) 93–100.
- [28] K. Hyun, M. Wilhelm, C. O. Klein, K. S. Cho, J. G. Nam, K. H. Ahn, S. J. Lee, R. H. Ewoldt, G. H. McKinley, A review of nonlinear oscillatory shear tests: Analysis and application of large amplitude oscillatory shear (LAOS), *Prog. Polym. Sci.* 36 (12) (2011) 1697–1753.
- [29] N. Roussel, Steady and transient flow behaviour of fresh cement pastes, *Cem. Concr. Res.* 35 (9) (2005) 1656–1664.
- [30] M. D. Ediger, C. A. Angell, S. R. Nagel, Supercooled Liquids and Glasses, *J. Phys. Chem.* 100 (31) (1996) 13200–13212.
- [31] F. d. Larrard, C. F. Ferraris, T. Sedran, Fresh concrete: A Herschel-Bulkley material, *Mater. Struct.* 31 (7) (1998) 494–498.
- [32] Y. Otsubo, S. Miyai, K. Umeya, Time-dependent flow of cement pastes, *Cem. Concr. Res.* 10 (5) (1980) 631–638.
- [33] F. Mahaut, S. Mokéddem, X. Chateau, N. Roussel, G. Ovarlez, Effect of coarse particle volume fraction on the yield stress and thixotropy of cementitious materials, *Cem. Concr. Res.* 38 (11) (2008) 1276–1285.
- [34] L. Struik, On the rejuvenation of physically aged polymers by mechanical deformation, *Polymer* 38 (16) (1997) 4053–4057.
- [35] M. Fourmentin, G. Ovarlez, P. Faure, U. Peter, D. Lesueur, D. Daviller, P. Coussot, Rheology of lime paste—a comparison with cement paste, *Rheol. Acta* 54 (7) (2015) 647–656.
- [36] D. Shmilovitz, On the definition of total harmonic distortion and its effect on measurement interpretation, *IEEE Trans. Power Del.* 20 (1) (2005) 526–528.
- [37] T. Loerting, V. V. Brazhkin, T. Morishita, Multiple Amorphous-Amorphous Transitions, in: S. A. Rice (Ed.), *Advances in Chemical Physics*, Volume 143, John Wiley & Sons, Inc., 2009, pp. 29–82.
- [38] Y. Cai, M. F. Thorpe, Floppy modes in network glasses, *Phys. Rev. B* 40 (15) (1989) 10535–10542.
- [39] O. B. Tsiok, V. V. Brazhkin, A. G. Lyapin, L. G. Khvostantsev, Logarithmic Kinetics of the Amorphous-Amorphous Transformations in SiO₂ and GeO₂ Glasses under High Pressure, *Phys. Rev. Lett.* 80 (5) (1998) 999–1002.
- [40] E. Principi, A. Di Cicco, F. Decremps, A. Polian, S. De Panfilis, A. Filippini, Polyamorphic transition of germanium under pressure, *Phys. Rev. B* 69 (20) (2004) 201201.
- [41] A. Pal, S. Gohil, S. Sengupta, H. K. Poswal, S. M. Sharma, S. Ghosh, P. Ayyub, Structural phase transitions in trigonal Selenium induce the formation of a disordered phase, *J. Phys. Condens. Matter* 27 (41) (2015) 415404.
- [42] A. Varshney, A. Sane, S. Ghosh, S. Bhattacharya, Amorphous to amorphous transition in particle rafts, *Phys. Rev. E* 86 (3) (2012) 031402.
- [43] M. Trulsson, B. Andreotti, P. Claudin, Transition from the Viscous to Inertial Regime in Dense Suspensions, *Phys. Rev. Lett.* 109 (11) (2012) 118305.
- [44] F. Boyer, É. Guazzelli, O. Pouliquen, Unifying Suspension and Granular Rheology, *Phys. Rev. Lett.* 107 (18) (2011) 188301.
- [45] A. Lemaître, J.-N. Roux, F. Chevoir, What do dry granular flows tell us about dense non-Brownian suspension rheology?, *Rheol. Acta* 48 (8) (2009) 925–942.